

**Emulated Radar Observations Of Near Updraft  
Vorticity In a Simulated Tornadic Supercell**

by

Austin W. Dixon

A thesis submitted in partial fulfillment of the requirements for the

degree of

Master of Science

(Atmospheric and Oceanic Science)

at the

UNIVERSITY OF WISCONSIN-MADISON

2019

## Acknowledgments

Working on this project has been the opportunity of a lifetime that was given to me by Dr. Leigh Orf. I started watching Leigh's presentations on YouTube as a sophomore in undergrad. I always wanted to be a part of his research but never imagined I actually would be. My dream has always been to study tornadoes and Leigh has made that possible for me. In addition to being a part of amazing research, Leigh has been an incredibly fun, encouraging, and constructive advisor. Any future student that has the pleasure of working in his lab will undoubtedly have a wonderful experience. Thank you again, Leigh, and I look forward to our future collaborations.

I would not have made it this far without the love and support of my family and friends. You have all been a crucial part of my educational career in both moral and financial support. Thank you for all of the phone calls during my time in Madison. I also want to thank my Wife's family for their support and being our escape during our time in graduate school. You provided us with some much-needed weekends away and plenty of home-cooked meals. It was always great to know that I had family close by if I was ever in need.

Finally, to my wife Natalie, thank you to the ends of the earth for your unwavering love, support, and encouragement. You are a shining light in the world and I am so fortunate to have you at my side. This paper is dedicated to you and the journey we have taken together to make it this far.

# Table of Contents

<b>Acknowledgments</b>	<b>i</b>
<b>Abstract</b>	<b>iii</b>
<b>1 Introduction</b>	<b>1</b>
<b>2 Data and Methods</b>	<b>5</b>
2.1 The Blue Waters Supercomputer .....	5
2.2 Base State Environment .....	5
2.3 RadSim Radar Emulator .....	6
2.4 Scanning Strategies .....	7
<b>3 Motivation &amp; Overview of the Streamwise Vorticity Current</b>	<b>9</b>
<b>4 Results</b>	<b>12</b>
4.1 Pre-Tornado Genesis .....	12
4.2 Tornado Genesis .....	13
4.3 Tornado Maintenance .....	15
<b>5 Discussion</b>	<b>17</b>
<b>6 Conclusion</b>	<b>21</b>
<b>Figures</b>	<b>23</b>
<b>Bibliography</b>	<b>43</b>

## Abstract

This paper analyzes techniques for identifying the Streamwise Vorticity Current (SVC) using Doppler radar. Techniques are analyzed using emulated radar images, in both PPI and RHI format, from the same 30m simulation of a tornadic supercell used in Orf et al. 2017. A more detailed investigation of the SVC is presented in an effort to better understand its influence on the storm. In the simulation of the May 24, 2011 El Reno, OK tornadic supercell, this feature develops more than 15 minutes prior to tornado genesis. As the low-level updraft intensifies, significant vertical shearing develops along the FFDB, and multiple misovortices form that train into the updraft similar to previously noted phenomena in field radar observations. This “misovortex train” (MVT) is likely due to the shearing instability along the FFDB. In this simulation, it appears that once vertical velocity in the updraft has reached a critical point, these vortices continuously conglomerate into a single, significantly more intense vortex that eventually becomes the tornado. This appears to be a direct result of the SVC’s influence on the storm.

# Chapter 1

## Introduction

In recent years, the so-called Streamwise Vorticity Current (SVC) has become a focal point of supercell thunderstorm research following the work of Orf et al. 2017. Orf et al. noted the SVC's potential role in tornado genesis for long-track, violent tornadoes through its interaction with the storm's updraft. Over the course of the last two decades, the rear-flank downdraft (RFD) has been a significant area of interest as a source of tornado genesis (Ludlam 1963; Fujita 1975; Burgess et al. 1977; Barnes 1978; Brandes 1981; Markowski et al. 2002; Markowski 2002a; Grzych et al. 2007; Hirth et al. 2008). It has been identified as an important source of tilting for baroclinically generated horizontal vorticity and near-surface vertical vorticity (Straka et al. 2007; Markowski et al. 2008; Markowski and Richardson 2014). Surges within the RFD have also been shown to transport angular momentum radially inward, surrounding the low-level mesocyclone and aiding in tornado genesis and maintenance (Marquis et al. 2012; Kosiba et al. 2013). However, the SVC exists within the forward-flank downdraft (FFD) on the cool side of the forward-flank convergence boundary (FFCB). Few studies have focused on the FFD region as a source of near surface vorticity (Klemp and Rotunno 1983; Rotunno and Klemp

1985; Brandes 1984). Shabbott and Markowski 2006 compared mobile Mesonet (Straka et al. 1996) observations of tornadic and nontornadic supercells, and concluded that it was in fact nontornadic supercells that possessed higher FFD baroclinicity and streamwise vorticity. However, they noted weaknesses in their observations including a lack of 3-dimensionality and low temporal resolution, which possibly led to less accurate depictions of the buoyancy fields.

The Rivers of Vorticity in Supercells (RiVorS) project, led by the National Severe Storms Laboratory (NSSL), was the first field experiment with the specific goal of identifying so-called “rivers of vorticity” in the FFD region of supercell thunderstorms. This project sought validation of apparent horizontal vorticity maxima in recent numerical simulations of supercells (e.g. Orf et al. 2017; Markowski et al. 2014) with their results through radar and mobile Mesonet observations. Mobile Mesonet observations in RiVorS found little evidence of the kinematic features noted in Orf et al. 2017. Both wind and temperature measurements were relatively homogenous along their transects with the exception of a few instances of weak temperature gradients around the mesocyclone. However, Doppler radar measurements during this experiment found encouraging signatures of a kinematic boundary similar to the SVC in RHI radial velocity data (Schueth 2018). While in-situ identification/verification of the SVC should be a continual focus moving forward, mobile Mesonet measurement methods may lack the 3-dimensionality and maneuverability necessary for proper sampling. This is especially true with respect to the vertical

extent of these measurements when the features of interest are several hundred meters tall and not necessarily at the surface. Therefore, the more viable method for analysis of the SVC may be through high-resolution mobile Doppler radars.

The SVC is a 3-dimensional flow feature and detecting it via radar derives challenges of its own given only 2-dimensional radar capabilities. Doppler radar detects only the component of the wind directed along the beam; flow components not read directly by the radar beam must be inferred (Desrochers and Harris 1996). Radar studies of diametrically opposed velocity couplets, such as radar presentations of mesocyclones, have been shown to represent circulatory flow in Plan Position Indicator (PPI) scans (Desrochers and Harris 1996). Similar radar presentations have been shown in Range Height Indicator (RHI) scans of gust fronts (Wakimoto 1982), where a circulation was shown to exist along the gust front through multiple phases of the storm's life cycle. The SVC in this simulation exhibits radar characteristics similar to rotors detected in gust fronts (see "Results"), which is promising for future goals of field detection. As mentioned previously, detection of the SVC with ground-based in-situ instruments may be challenging due to its elevated nature. However, the SVC still exists at relatively low altitude, residing below 1 km along much of its length. Even advanced high-resolution mobile Doppler radars such as the Rapid-scanning X-band Polarimetric radar (RaXPoL; Pazmany et al. 2013), and the Atmospheric Imaging Radar (AIR; Isom et al. 2013) often encounter situations where low-altitude features such as atomized precipitation in the weak-echo

region (WER) are poorly resolved in PPI scans (Kurdzo et al. 2017). Nonetheless, these radars represent state-of-the-art technology and provide the greatest opportunity for studying features such as the SVC.

Orf et al. 2017 modeled a complete supercell at 30-m isotropic resolution that produced a long-track, violent tornado with sustained winds exceeding 90 m/s (EF-5 threshold). One of the primary discoveries of this work was the aforementioned SVC, which appeared to influence the strength of the low-level updraft and possibly aid in tornado genesis. In an effort to present field researchers and operational forecasters with more information about the SVC, this paper involves further investigation of the SVC through quantitative analyses of the simulation data from Orf et al. as well as emulated radar scans in both PPI and RHI formats. This paper serves two purposes: first, to further investigate the relationship between the SVC and its parent supercell and, second, to provide some insight as to what the SVC might look like in PPI/RHI radar presentations prior to, during, and following tornado genesis. Two approximate radar resolutions are used for PPI scans: operational NEXRAD WSR-88D, and RaXPol (see “scanning strategies”). RHI scans are performed at approximate RaXPol resolution since mobile research radars typically utilize this technique. The apparent enhancement of the low-level updraft is the primary focus of the quantitative analyses. Basic radar data, including reflectivity and radial velocity, are the main focus for the emulated

presentations. Multiple facets of the SVC appear visible in these radar data in both scanning formats.

## **Chapter 2**

### **Data and Methods**

#### **2.1 The Blue Waters Supercomputer**

Blue Waters (Bode et al. 2013; Kramer et al. 2014) is a massively parallel computer containing over 22,500 compute nodes, each containing 16 floating-point processing cores and 64 GB of memory. It is located at the University of Illinois Urbana-Champaign in the National Center for Supercomputing Applications. The simulation discussed in this paper was conducted on a 2,200 x 2,200 x 380 grid with 30-m grid spacing in 3-dimensions, which produced around 100 TB of data output when saving data frequently (Orf et al. 2017).

#### **2.2 Base State Environment**

This study uses Cloud Model 1 (CM1) version 16, a three-dimensional, non-hydrostatic model designed for idealized studies of atmospheric phenomena (Bryan and Fritsch 2002). The sounding and wind profile used for model

initialization was taken from the 1-h Rapid Update Cycle (RUC; Benjamin et al. 2004) model forecast (Fig. 1). The sounding was located off the right-flank of the supercell thunderstorm that produced a long-track EF5 tornado on May 24, 2011 near El Reno, Oklahoma (Houser et al. 2015). The sounding shows large amounts of conditional instability, with surface-based convective available potential energy (CAPE) of  $4,893 \text{ J kg}^{-1}$ . This is paired with a strong 0-6-km bulk wind difference near  $27 \text{ ms}^{-1}$ , a magnitude in the upper quartile for shear associated with supercell thunderstorms (Houston et al. 2008). Low-level moisture and kinematics lie in the lower and upper quartiles for supercells producing significant ( $\geq \text{EF2}$ ) tornadoes, respectively, with an LCL of 528 m and 0-1-km storm-relative helicity (SRH) of  $371 \text{ m}^2 \text{ s}^{-2}$  (Thompson et al. 2003).

## 2.3 RadSim Radar Emulator

For this study it was necessary to develop radar emulation software capable of processing high-resolution simulation data and converting it to a polar coordinate grid. RadSim converts reflectivity to a polar coordinate grid at user-desired specifications, for both Plan Position Indicator (PPI) and Range Height Indicator (RHI) “scanning.” The 3-dimensional wind vectors are converted to radial velocity on the same polar coordinate grid, again in both PPI and RHI. This software does not *simulate* a radar image by using a true

simulated beam of radiation, but rather emulates an approximate radar image. The user has the ability to interactively define the radar location, range, range step, azimuth, azimuth step, and elevation. Range step and azimuth step are the intervals at which a scan is made (e.g. azimuth step = 1°). Defining these variables creates bins resembling those seen in real radar images. Decreasing the azimuth step and range step will create smaller bins (i.e. a higher-resolution image). Since this software is merely an emulator, the curvature of the Earth is not accounted for, and there are no issues with range folding, ground clutter, biological returns, anomalous propagation, terrain, side-lobing, or other erroneous returns. Consequently, the radar images presented in this paper may contain features not visible with real radars due to the aforementioned errors or other sensitivity issues.

## 2.4 Scanning Strategies

One of the primary targets of this study was the SVC, and its presentation on radar. Images from the simulation were chosen at critical time steps (namely prior to, during, and after tornado genesis) and then converted to PPI and RHI images using RadSim. WSR-88D, and RaXPOL (Pazmany et al. 2013) were the two approximate RadSim resolutions chosen for attempting to identify the SVC (Table 1). All RHI scans presented hereafter are at approximately RaXPOL

resolution since RHI cross-sections are typically performed with research radars. Radar locations were varied to test multiple scanning angles, especially with regards to RHI scans. Priority was then given to radar locations and azimuth angles that showed possible evidence of the SVC. All emulated RHI scans presented in this study used a minimum zenith angle of  $0^\circ$  and a maximum angle of  $20^\circ$ . All emulated PPI scans used a constant zenith angle of  $0.5^\circ$ . While WSR-88D radars are typically run at fixed settings, RaXPol can be run at different resolutions (range/azimuth increments) based on user input. While RaXPol is capable of range-gate spacing of 7.5m, running the emulator at this resolution is almost no different from viewing the raw simulation data, especially when viewing reflectivity. It should also be noted that in rapid-scan mode (a  $10^\circ$  elevation full  $360^\circ$  volume scan every 20 seconds), RaXPol is only able to maintain azimuth increments of  $1^\circ$ . The values shown below in Table 1 were determined to be the best settings for analyzing the SVC under semi-realistic radar conditions.

### WSR-88D Emulator Settings

Elevation Angle	0.5°
Azimuth Increment (Step)	1°
Range Increment (Step)	250 m

### RaXPol Emulator Settings

Elevation Angle	0.5°
Azimuth Increment (Step)	1°
Range Increment (Step)	30 m

**Table 1.** Elevation, Azimuth Increment, and Range Increment settings for the WSR-88D and RaXPol radar emulators, respectively.

## Chapter 3

### Motivation and Overview of the Streamwise

### Vorticity Current

The SVC is defined by Orf et al. 2017 as “a persistent tube of streamwise vorticity located along the FFDB that flows rearward along the FFDB and

eventually upward into the updraft.” In order to perform a more quantitative analysis of this feature, a more rigorous definition of the SVC is presented hereafter.

In the simulation of the May 24, 2011 El Reno, OK tornadic supercell, this feature develops more than 15 minutes prior to tornado genesis. The most notable effect of the SVC is an apparent enhancement of the low-level updraft. Vertical velocity increases by approximately 10 m/s (Fig. 2) and the updraft itself lowers by more than 500m (Fig. 3) during this time. This lowering and strengthening likely results in a positive feedback that intensifies low-level vorticity, including that within the SVC, further strengthening the low-level updraft and vorticity itself (Rotunno and Klemp 1982). Using isosurfaces, a lobe of -15 hPa pressure perturbation can be seen extending horizontally in the direction of the SVC (Fig. 2). The increase in vertical velocity takes place concurrently with this pressure perturbation. When this -15 hPa pressure perturbation becomes visible, the SVC is most clearly defined, with streamwise vorticity maxima of  $0.25 \text{ s}^{-1}$  and growing. However, lowering of the low-level updraft begins several minutes prior to the primary pressure falls associated with the SVC. At the time when low-level updraft lowering begins, streamwise vorticity maxima along the SVC are lower, on the order of  $0.1 \text{ s}^{-1}$ . It is this magnitude of vorticity, which becomes visible ~45 minutes into the simulation, that presents the most persistent signature prior to the later strengthening. For the purposes of this paper, the SVC is further defined as a persistent tube of

streamwise vorticity, enclosed by an isosurface of approximately  $0.1 \text{ s}^{-1}$ , located along the FFDB that flows rearward along the FFDB and eventually upward into the updraft. It is observed in the simulation that once the SVC obtains a magnitude of approximately  $0.1 \text{ s}^{-1}$ , the low-level updraft begins strengthening and lowering to the ground.

A staple of the SVC in this simulation is the apparent presence of a vortex sheet along the southern side of the boundary. As the low-level updraft intensifies, significant vertical shearing develops along the FFDB, and multiple misovortices form that train into the updraft (Fig. 4) similar to the phenomena observed by Snyder et al. 2013. For brevity this phenomenon is hereafter referred to as the “misovortex train” (MVT). The formation of the MVT is likely due to the shearing instability along the FFDB (Markowski and Richardson 2014). In this simulation, it appears that once vertical velocity in the updraft has reached a critical point, these vortices continuously conglomerate into a single, significantly more intense vortex that eventually becomes the tornado. This appears to be a direct result of the SVC’s influence on the storm; the motivation for this paper is analyzing techniques for identifying the SVC and/or subsequent MVT via Doppler radar.

## Chapter 4

### Results

#### 4.1 Pre-Tornado Genesis

Emulated reflectivity presentations at both RaXPol and WSR-88D resolution show a notable gradient in precipitation along the FFDB during in the weak echo region (WER), and following, the formation of the SVC (Fig. 5). At this time step, this signature in reflectivity is collocated with the zero isodop in ground-relative radial velocity (GRV) along the FFDB, as well as the SVC once it has formed (Fig. 6). There is no obvious signature to suggest an SVC in PPI scans prior to the moments leading up to tornado genesis. However, horizontal vorticity tubes in the forward flank precipitation core (FFPC) are somewhat resolved in the high-resolution scans (Fig. 6). There is some evidence that these are detectable with research radars (Wood et al. 2018), but their presence and magnitude possibly varies significantly between storms. The impact of their associated vorticity on the storm and subsequent tornado is not fully understood at this time and is beyond the scope of this paper.

RHI scans perpendicular to the SVC (radar bisects the SVC at an angle of  $90^\circ$ ) (Fig. 7) show strong outbound flow from the warm sector rising over strong inbound flow from the FFPC in storm-relative radial velocity (SRV), suggesting

significant shearing in this region. Reflectivity shows a 2.5 km tall reflectivity billow that bends back toward the FFPC, which is collocated with the zero isodop. Figure 8 is a horizontal cross section of model streamwise vorticity in the same location as that of Figure 8. Widespread values of streamwise vorticity magnitudes  $0.07 \text{ s}^{-1}$  and greater are present at this time with a local maximum of  $0.20 \text{ s}^{-1}$  near the upper region of the SVC. The evolution of this signature closely resembles the gust front structure presented by RKW theory (Rotunno et al. 1988) and Wakimoto 1982, which suggests the likelihood of a rotor along this boundary. This RHI characteristic appears to be the telltale signature of the SVC in this simulation. The orientation of the SVC is nearly meridional with respect to the domain at this time, which is an important note for future time steps.

## 4.2 Tornado Genesis

Tornado genesis occurs in this simulation at time 3830 with several notable radar characteristics ongoing in the moments leading up to that time. Possibly the most notable and useful is the prominent signature of the MVT in PPI scans (Fig. 9 & Fig. 10a, 10b), particularly in SRV. Reflectivity scans again show a prominent gradient in reflectivity along the FFDB in the WER that is collocated with the SVC. As discussed in previous sections, special circumstances

may be required for actual radars to detect this feature since much of it exists below 1 km. However, it is worth noting this seemingly significant feature as radar technology continues to improve. In this simulation, this reflectivity signature seems to be the only obvious evidence of the SVC in PPI scans. When viewing SRV at location 2 (Fig. 10b), the MVT becomes increasingly apparent in the moments between 3610 and the time of tornado genesis at 3830. Several small-scale couplets denoting aforementioned misovortices can be seen training into the updraft region at both RaXPol and WSR-88D resolution. In terms of forecasting utility drawn from this simulation, this signature is likely the most significant as it is an obvious pre-cursor to tornado genesis.

RHI scans perpendicular to the SVC at this time (Fig. 11) show a similar signature to that of time 3610, with perhaps a slightly more organized outbound region. Given the increasing updraft strength in the moments leading up to tornado genesis, a more organized inflow (outbound) signature is to be expected. The only other notable change at this time step is the decrease in height of the reflectivity billow by nearly 1 km. This is possibly a result of the stronger inflow at this time but the exact cause is unknown.

The cross section of model streamwise vorticity at this time (Fig. 12) shows relatively similar overall magnitudes, with widespread areas of over  $0.07 \text{ s}^{-1}$  and local maxima of over  $0.20 \text{ s}^{-1}$ . However, at this time the SVC appears to have become more bent back towards the FFPC in a similar shape to the velocity scan in Fig. 11, possibly due to the stronger inflow as mentioned before.

### 4.3 Tornado Maintenance

The tornado maintenance phase is analyzed hereafter at time 5550, approximately 1720 time steps after tornado genesis. At this time the tornado has taken on a two-celled structure (Rotunno et al. 2013) with a central axis downdraft extending to the surface. Radar presentation shows a notable evolution in storm structure with a much more narrow band of reflectivity extending around the rear-flank of the storm (Fig. 13). This is accompanied by a more pronounced WER and a defined reflectivity gradient extending from the FFPC into the updraft region, co-located with the SVC. Both WSR-88D and RaXPoI resolution scans of reflectivity show relatively similar features at this time step. However, due to factors mentioned in Chapter 2, section 3, the visibility of SVC features in the WER in WSR-88D resolution is likely overestimated.

Perhaps the most significant result in terms of real storm comparison comes when viewing radial velocity scans at this time step in the simulation. Emulated scans at both WSR-88D and RaXPoI resolution show a significant jet along the FFCB that extends into the updraft region and ongoing tornado (Fig. 14). It is known that the SVC exists at this time and location in the simulation, but it should be noted that this signature does not necessarily suggest rotational

flow. However, recently an EF-2 tornado occurred in near Paducah, Kentucky in close proximity to the KPAH WSR-88D radar site. Radial velocity scans of the Paducah storm show a similar signature to that of the emulated radar scans at time 5550 when the emulated radar is placed at a similar location (Fig. 15). To the author's knowledge, this is one of the best instances of a possible SVC detection by operational radar at the time of this paper. While this does not guarantee that the Paducah storm featured an SVC, the simulated storm has an SVC and both images show very similar features. This is a promising result for future investigation of the SVC with Doppler radar.

RHI scans through the SVC at this time step show a signature that is interestingly less noisy in both reflectivity and SRV (Fig. 16). The reduction in the reflectivity can be attributed to the significant lack of hydrometeors in the WER in comparison to earlier time steps. However, there is also a lowering of the reflectivity billow of 1 km at this time. This is possibly due to the decrease in both inbound and outbound velocities by over 20 m/s along this boundary, resulting in less of the gyre effect that would produce the upward motion of hydrometeors noted in previous time steps. If the gyre along the FFCB has decreased at this time, it could suggest a weakening of the SVC.

Again, in contrast to previous time steps, the cross-section of model streamwise vorticity at time 5550 has evolved quite drastically (Fig. 17). Qualitatively speaking, it is much less coherent and extends higher into the storm. The close resemblance of the cross sections to Kelvin-Helmholtz billows in

previous time steps is no longer apparent. Streamwise vorticity magnitudes during this time remain largely the same, with widespread areas of  $0.07 \text{ s}^{-1}$  and local maxima of over  $0.20 \text{ s}^{-1}$ . The SVC as it is defined in this paper is still present, but its presentation has clearly deviated from the moments leading up to tornado genesis.

## Chapter 5

### Discussion

Detection of the SVC with operational NEXRAD radars is going to be hard to come by in most circumstances. The greatest hope for this happening is a supercell passing extremely close to the radar as in the case of the Paducah, Kentucky storm. If the SVC is in fact important to tornado genesis, as it appears to be in these simulations (though it has not been proven at this time), the ultimate goal would be early detection resulting in advanced warnings. Unfortunately few supercells pass closely to operational radars, and the likelihood of one passing at the opportune time is low in most cases. The most fruitful radar-based pursuit of the SVC looks to be in the research sector for the time being. The high-resolution, mobile capabilities of research radars will give scientists a substantial advantage over NEXRAD. One of the primary challenges of identifying the SVC via radar is its 3-dimensional nature. The hallmark of

the SVC is the helical flow (Orf et al. 2017), which, in the model, makes at least one full revolution as it begins tilting into the updraft. Consequently, the true nature of the SVC is difficult to diagnose with the 2-dimensional data provided via radar.

It seems the most reliable radar presentation of the SVC is that of the aforementioned “over-under” signature noted in previous RHI scans, and the MVT, which is visible in PPI scans, that occurs in the moments leading up to tornado genesis. The over-under signature is commonly associated with radar scans of gust fronts in Mesoscale convective systems (MCS), where it is known that rotor-like features exist. When designing a field project for studying the SVC, it would be crucial to collect both PPI and RHI radar scans simultaneously in order to identify as many features as possible that could point to its presence. PPI scans seem to provide the best data when centered in line with, or slightly north of, the storm motion with the WER being the primary focus. Radial velocity scans appear to be the more viable option in PPI format, however, radar operators should clearly use their best judgment in determining the best techniques based on current knowledge of the SVC. Based on the ability to capture the horizontal shear (“over-under”) signature across the SVC, RHI cross-sections appear to be the best strategy for scanning the SVC itself and attempting to visualize its three-dimensional characteristics. Based on this paper, radar operators would want to transect the SVC as perpendicular as possible to retrieve the most information about its evolution. This would allow

for non-diluted estimations of inbound and outbound velocities across the FFCB. However, the goal of a perpendicular scan brings up a challenge of determining the SVC's exact location and orientation. Prior to and during tornado genesis in this simulation, the SVC is oriented mostly north-south. As the tornado forms and begins to intensify, the SVC begins to re-orient to the northeast and remains so throughout much of the tornado's life cycle. The reason for why this happens in the simulation and how to predict it is not understood at this time. Knowing the orientation of the SVC at a given time in a real storm would require real-time knowledge of the flow field within the weak-echo region. Given the obvious danger of this region in tornadic storms, it is often poorly sampled. One possibility would be careful observation of the tail cloud that feeds into the low-level updraft. This feature is co-located with the SVC in this simulation. However, it is not known at this time if tail clouds are synonymous with SVCs. This in itself could be a fruitful pursuit in future research.

The SVC as it is defined in this paper begins interacting with the updraft shortly before time 3600. There is a non-linear feedback process that unfolds as this takes place. Figure 18 shows the area over which vertical velocity,  $\frac{dw}{dz}$ , and streamwise vorticity were averaged from time 3000 to 4600. There is a marked lowering of  $\sim 15$  m/s vertical velocity isosurface by over 500m beginning near the time 3600 prior to tornado genesis at time 3830 (Fig. 19). Simultaneously, the same rapid increase in  $\frac{dw}{dz}$  can be seen in the lowest 1 km (Fig. 20), suggesting

significant vertical acceleration near the ground. And finally, streamwise vorticity increases in both magnitude and height during this same time (Fig. 21). It remains to be seen which of these quantities is the causal factor, if any. Regardless, these plots suggest a feedback process that eventually culminates in a tornado. Recall, the MVT is present during the time that these enhancements are taking place. When viewing supplemental animations provided in Orf et al. 2017, it is clear that these misovortices along the SVC eventually become the tornado. However, the MVT does not conglomerate randomly into a tornado as it reaches the updraft; the strength of the updraft seems to reach a critical point that drives vertical vorticity in the area to converge and coalesce (Orf et al. 2017). There appears to be no identifiable “trigger” for tornado genesis in this particular simulation. However, there is no intent to make this claim for all tornadoes. Considering that violent tornadoes are estimated to make up over 70% of all tornado-related fatalities, further investigation of this phenomenon is undoubtedly warranted if this continues to be the case in future simulations. There is years of future work to come from this data, but as the SVC continues to be an area of focus, the resultant MVT and its own effects on tornado genesis should be a topic of thorough discussion. Discerning the environments that result in supercells having an SVC, that also produce an MVT, could be a significant step forward in forecasting violent tornadoes.

## Chapter 6

### Conclusion

In this study a brief quantitative and qualitative analysis of the SVC was presented through model derived data fields and emulated radar scans. It was determined that the SVC's interaction with the storm appears to have an impact on its evolution through enhancement of the low level updraft. Near-updraft averaged model data fields, including streamwise vorticity, vertical velocity, and vertical acceleration  $\frac{dw}{dz}$ , all experience a marked increase once the SVC reaches a spatially average magnitude of at least  $0.1 \text{ s}^{-1}$  near time 3600. These enhancements, in concert with the SVC's resultant MVT, seem to reach a critical point where the strength of the low-level updraft results in a conglomeration of these misovortices, which eventually become the tornado. Evidence of the SVC, including misovortices within the MVT, are visible on the emulated PPI scans that have been presented, especially those at high resolution. RHI cross-sections through the SVC show characteristics of a rotor similar to those presented in previous radar studies of gust fronts. The optimal RHI scanning strategy of the SVC appears to be a perpendicularly oriented beam, which can be achieved by aiming the radar through the WER, approximately perpendicular to the storm motion. Evidence of a kinematic boundary resembling the SVC has been recently noted on operational radar scans of a tornadic supercell near Paducah, Kentucky. This result is encouraging for possible operational detection of this

feature, but it will likely continue to be a very rare and conditional instance.

Until operational radar technology receives an upgrade to both temporal and spatial resolution capabilities, mobile research Doppler radars are better suited for analysis of the SVC. Further investigation of the SVC in field research is needed for a better understanding of its role in the behavior of supercell thunderstorms and tornadoes.

## Figures

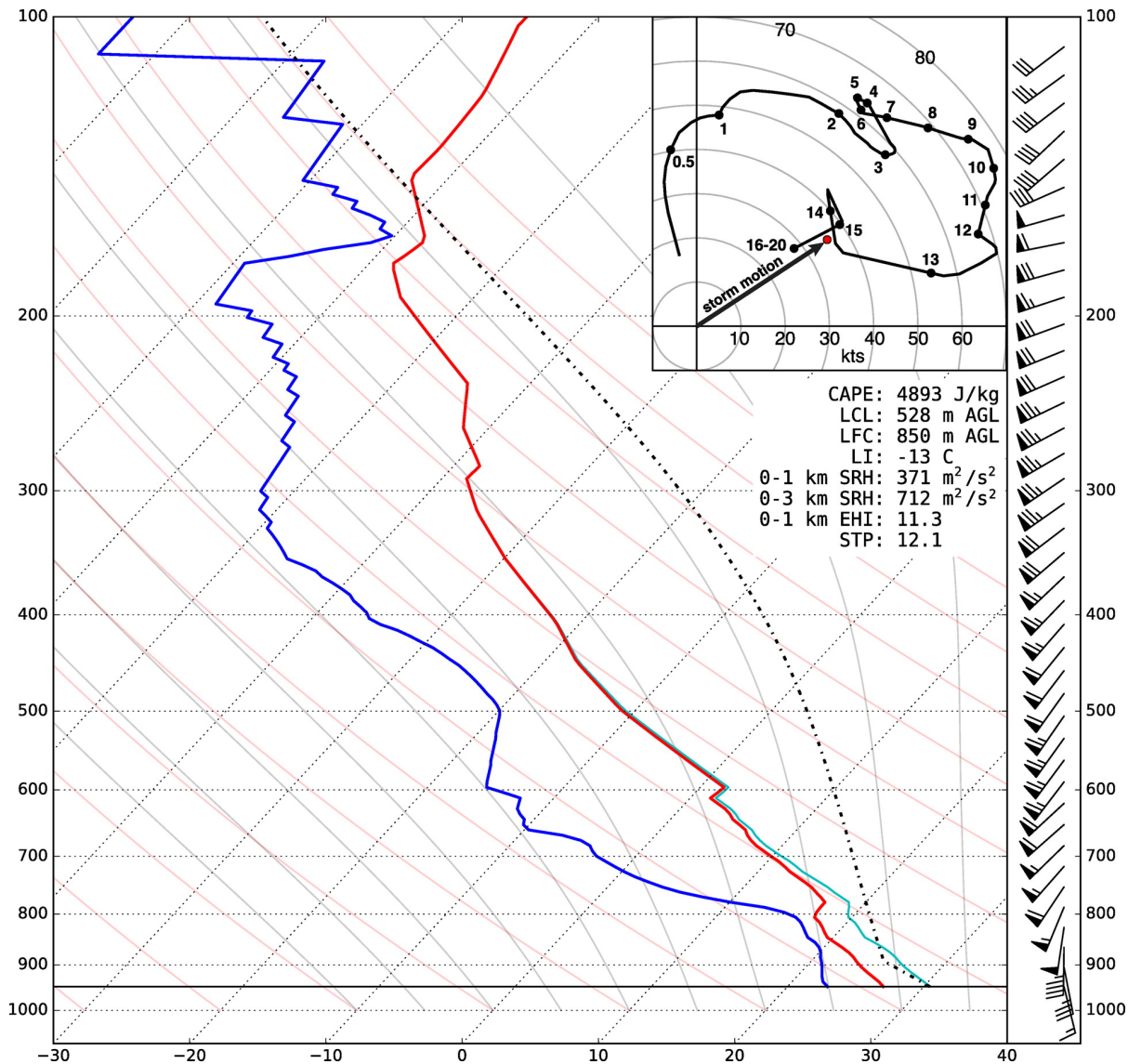


**Figure 1.** Sounding taken from the 1-hr RUC forecast off the right flank of the May 24, 2011 supercell that produced a long track EF5 tornado near El Reno, Oklahoma. Significant levels were calculated using the surface-based parcel and CAPE was calculated using the virtual temperature correction. Wind and hodograph values are shown in Knots.

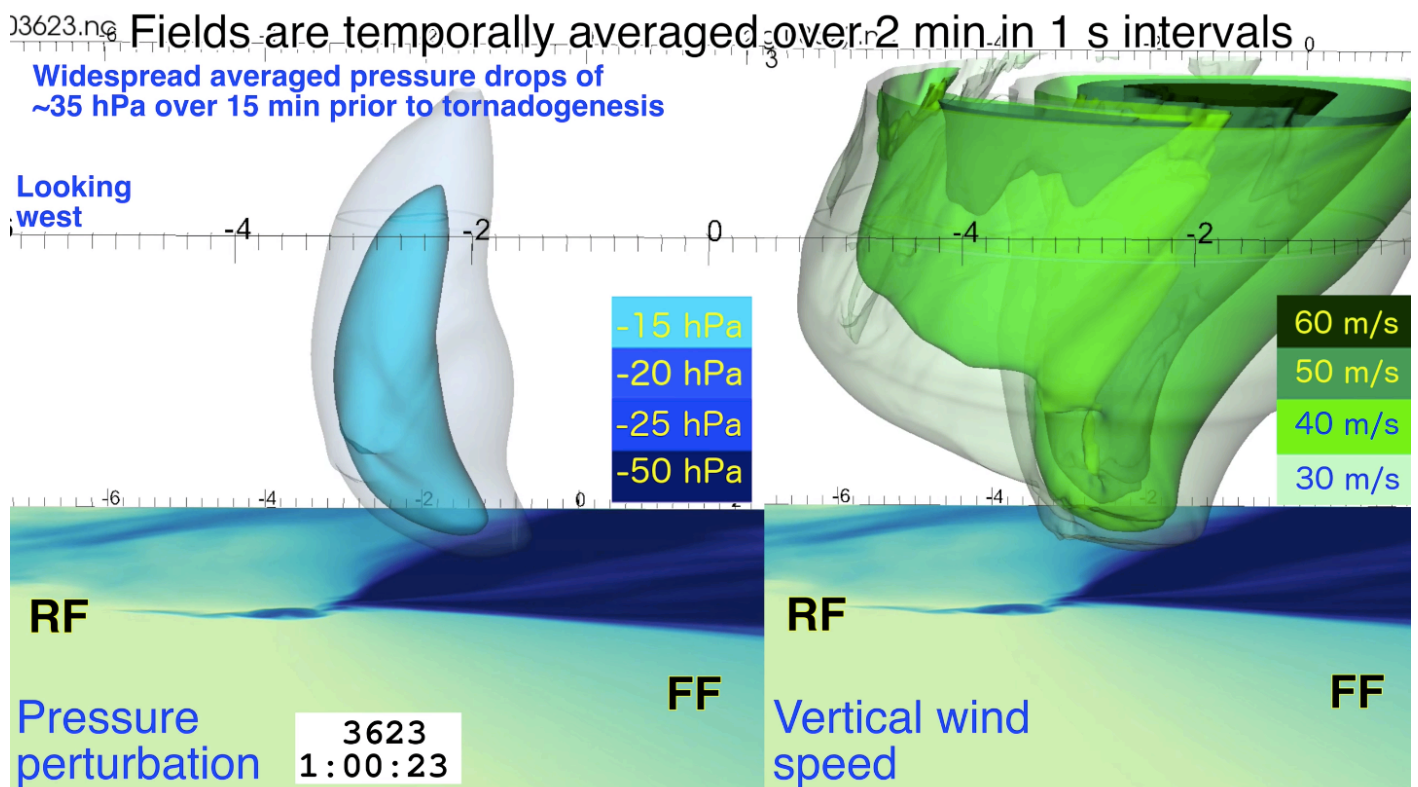


**Figure 2.** 2 minute temporally averaged volume rendering of pressure perturbation (left; blue) and vertical wind speed (right; green) courtesy Dr. Leigh Orf. 2-dimensional temperature perturbations are shown at the surface.

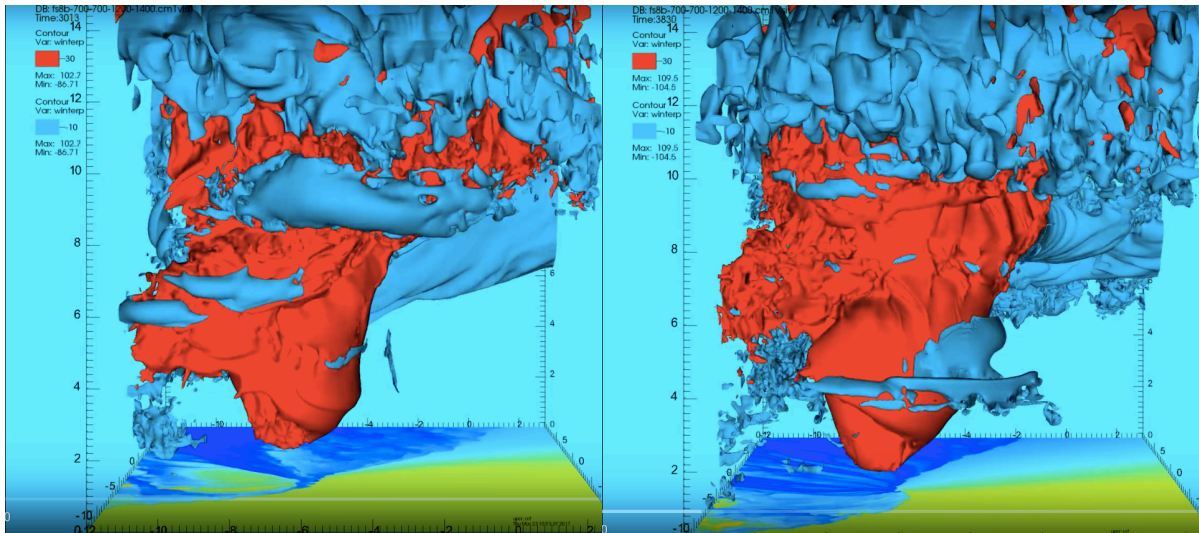


**Figure 3.** Volume rendering of  $30 \text{ m s}^{-1}$  (red) and  $-10 \text{ m s}^{-1}$  (blue) vertical velocity isosurfaces courtesy Dr. Leigh Orf. The left image, at time 3013, is the approximate time at which the SVC becomes present as it is defined in this paper. The right image, at time 3830, is the approximate time of tornado genesis.

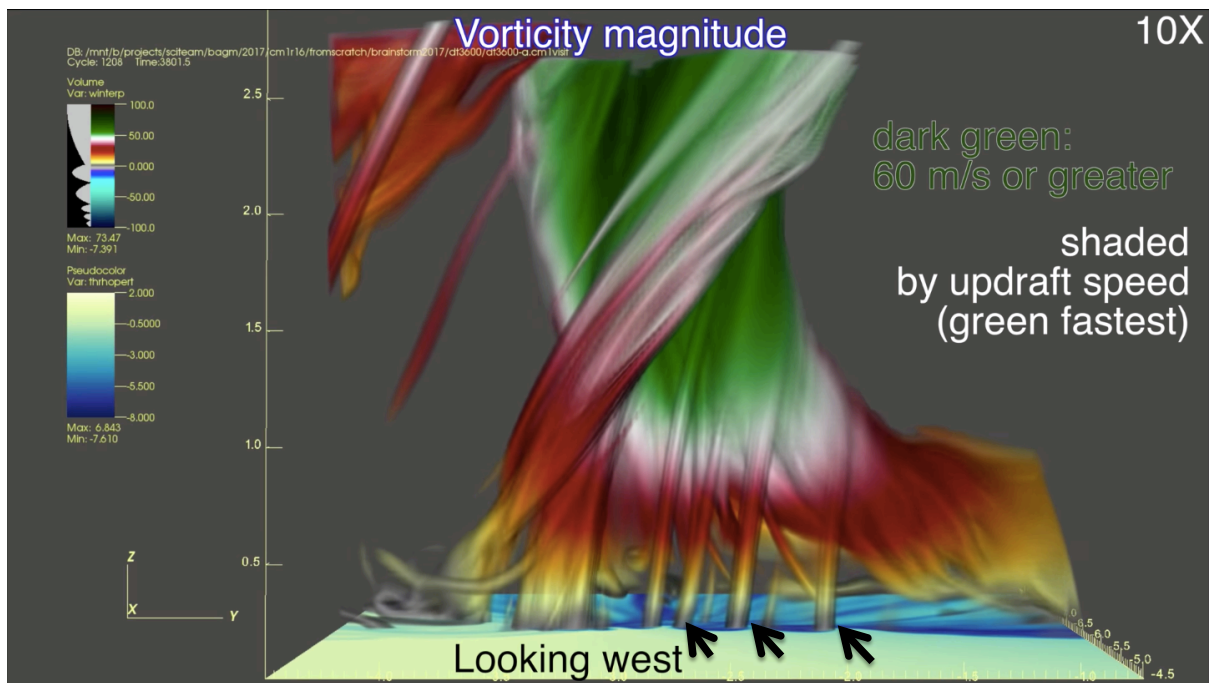


**Figure 4.** Vorticity magnitude shaded by updraft speed courtesy Dr. Leigh Orf. Black arrows denote locations (not all) of misovortices along the FFDB.

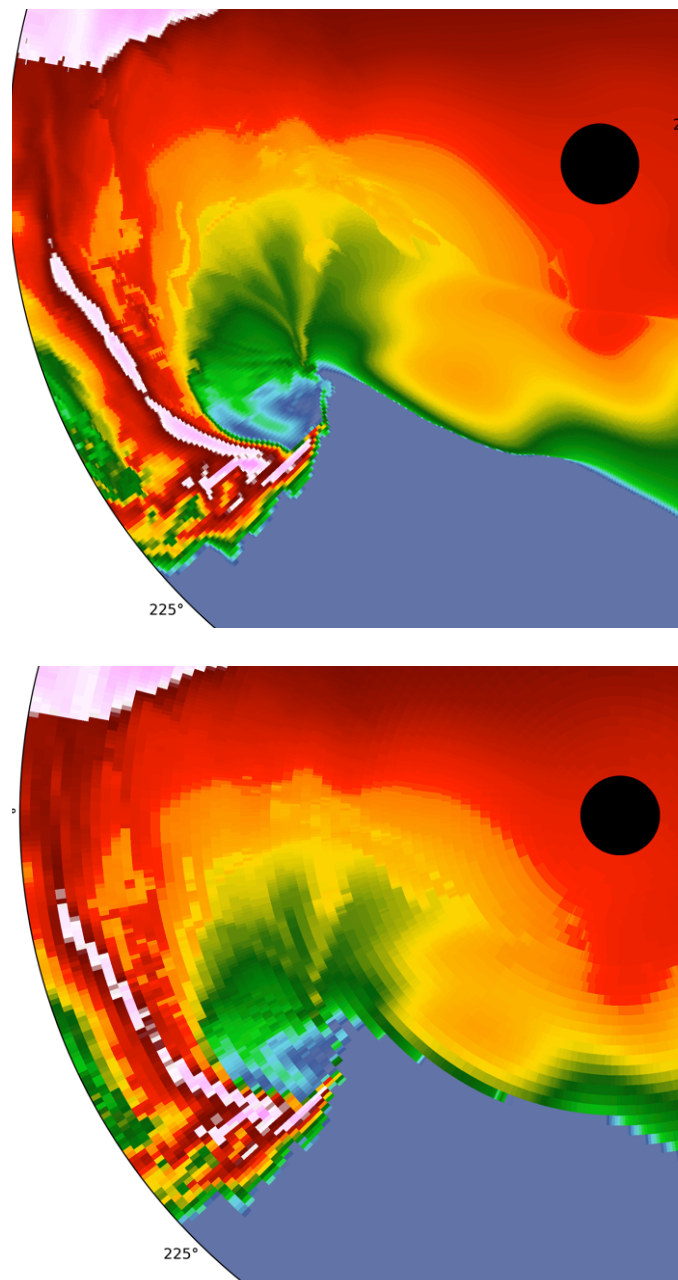


**Figure 5.** PPI reflectivity scans at time 3610 at approximate RaXPol (upper) and WSR-88D (lower) resolution. Black dot denotes radar location and black numbers leading away from the radar denote distance in kilometers from radar.

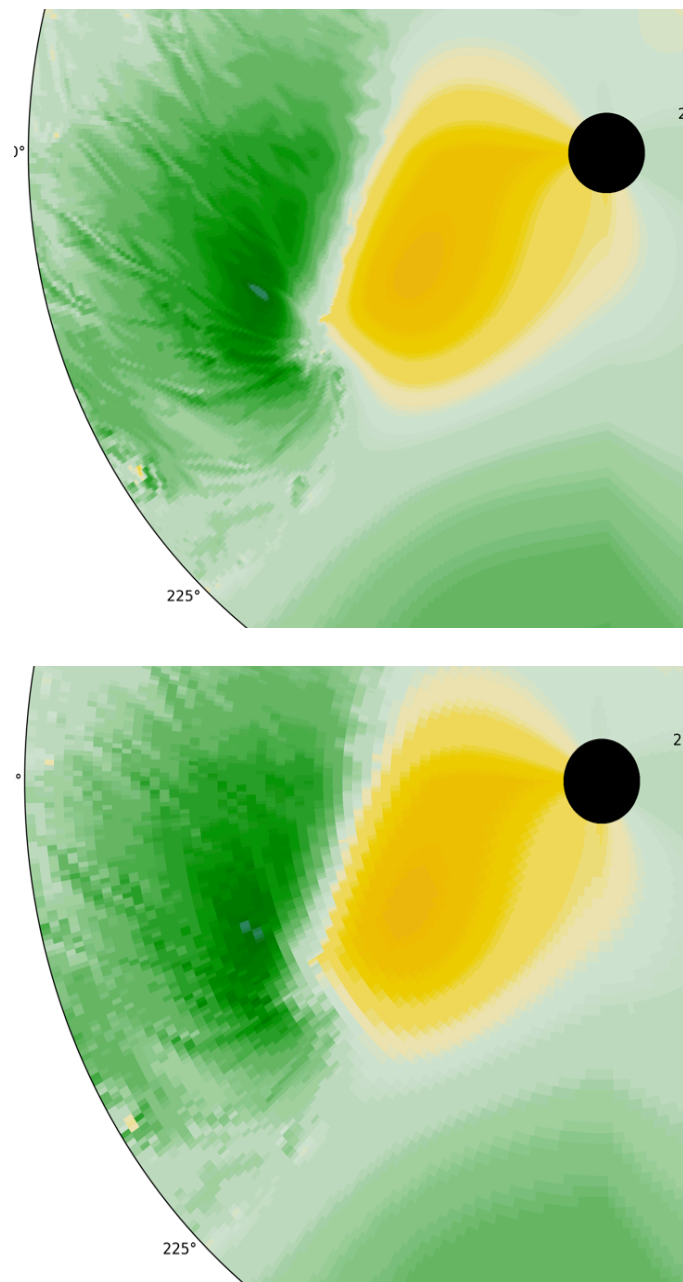


**Figure 6.** PPI scans of GRV at time 3610 at approximate RaXPol (upper) and WSR-88D (lower) resolution.

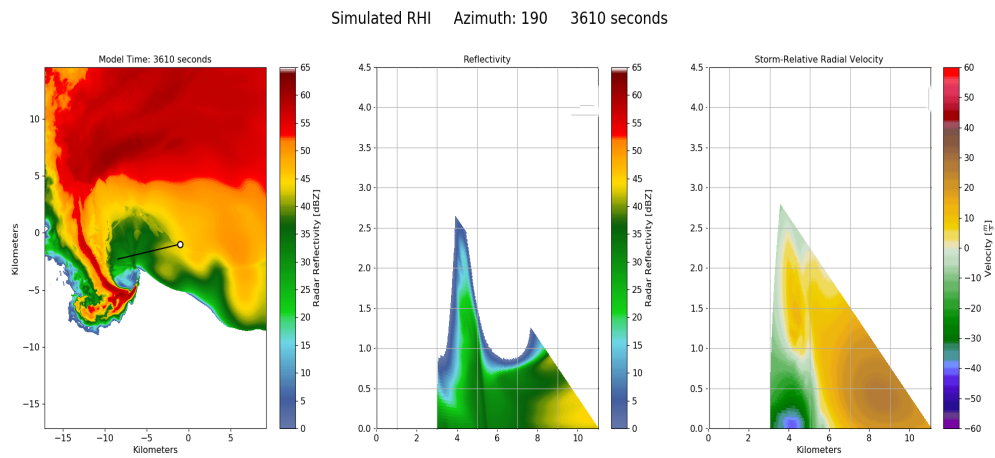


**Figure 7.** RHI scans perpendicular to the SVC at time 3610. Left panel shows location of RHI cross section (black line), center panel (a) shows horizontal cross section of reflectivity along RHI, and right panel (b) shows horizontal cross section of storm-relative radial velocity along RHI.

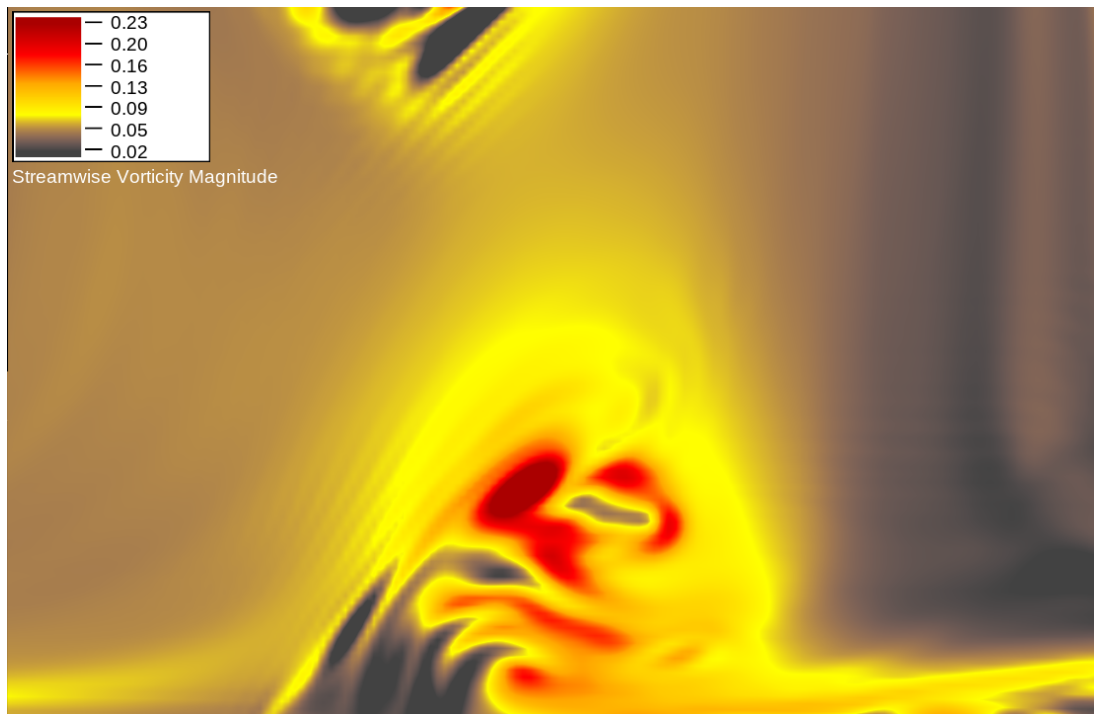


**Figure 8.** Horizontal cross section of model streamwise vorticity along the black line shown in figure 7.

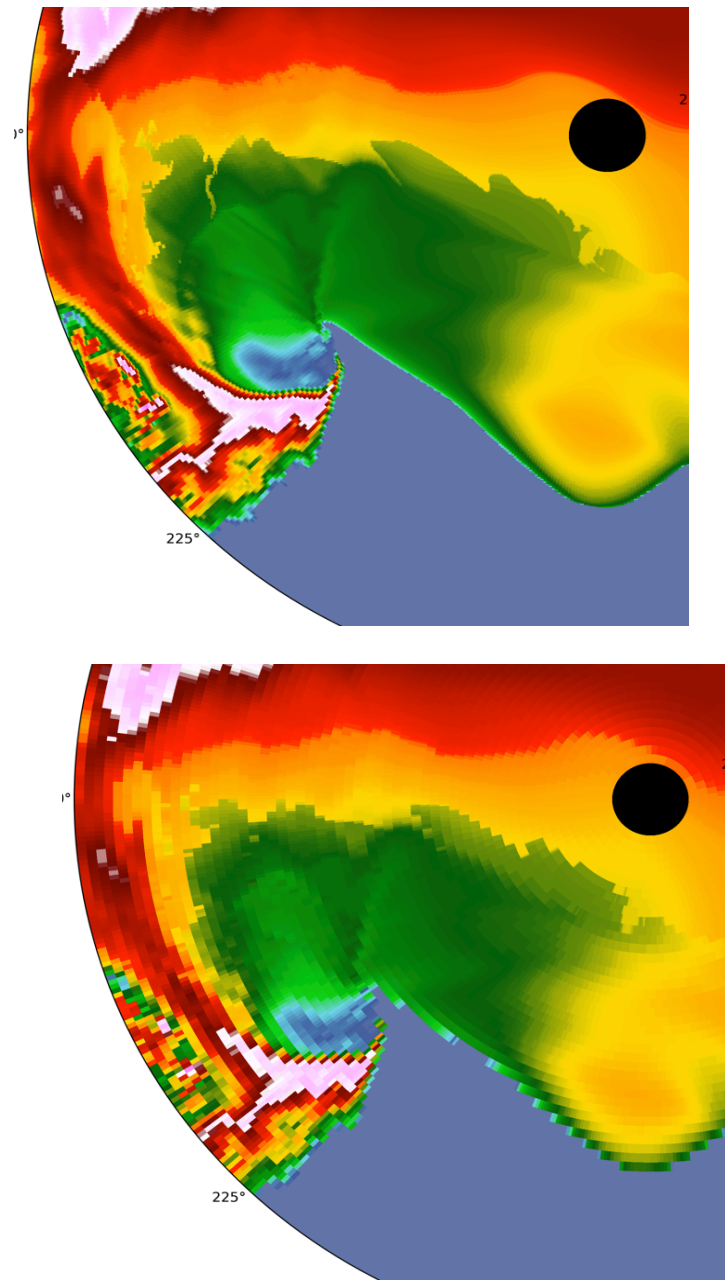


**Figure 9.** PPI scans of reflectivity at time 3830 at approximate RaXPol (upper) and WSR-88D (lower) resolution.

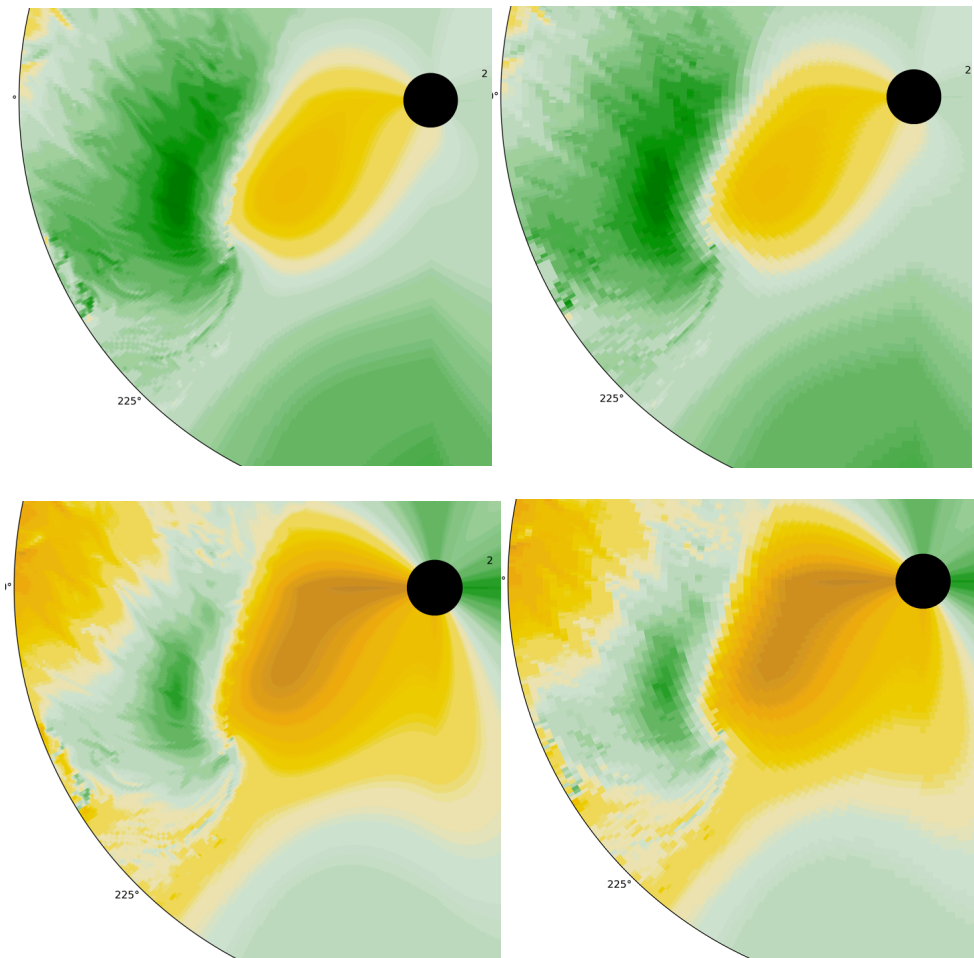


**Figure 10a.** PPI scans of GRV (top) and SRV (bottom) at time 3830 at approximate RaXPol (left) and WSR-88D (right) resolution.

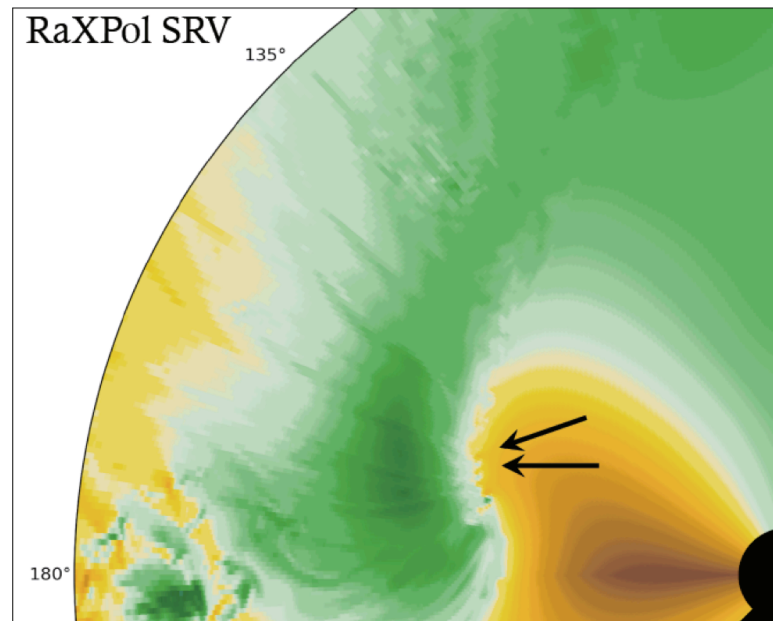


**Figure 10b.** RaXPoI PPI SRV at radar location 2 at time 3830. Black arrows denote location of misovortices in the MVT.

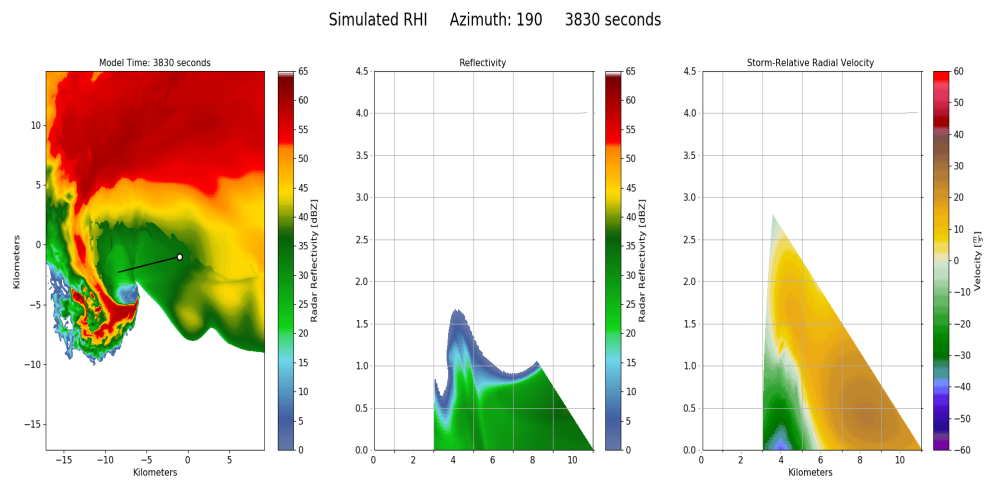


**Figure 11.** RHI scan perpendicular to the SVC at time 3830. Panels shown are same as figure 7.

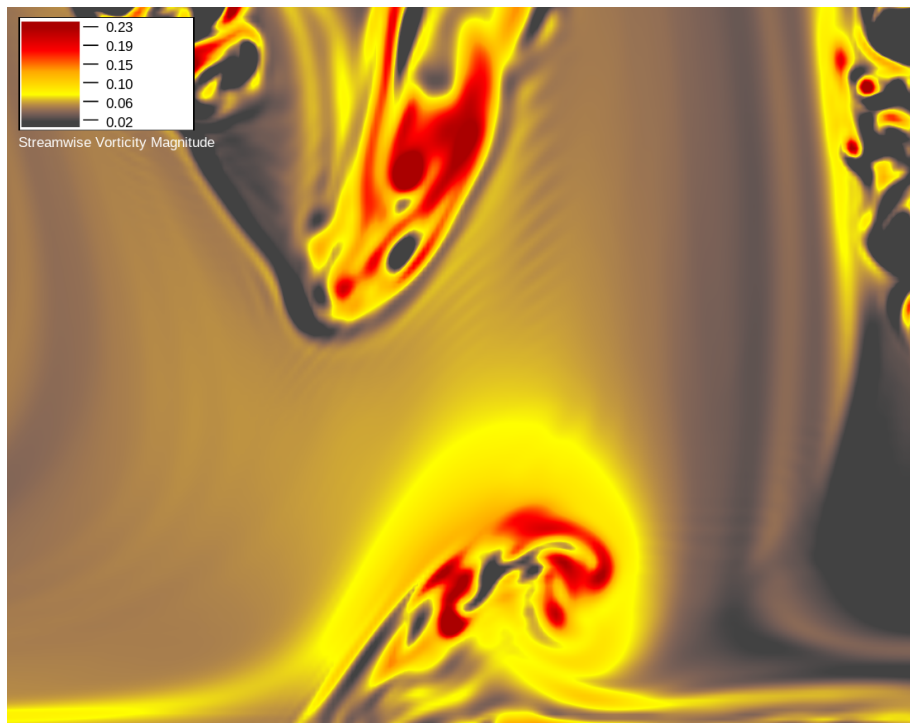


**Figure 12.** Horizontal cross section of model streamwise vorticity at time 3830 along the black line shown in figure 11.

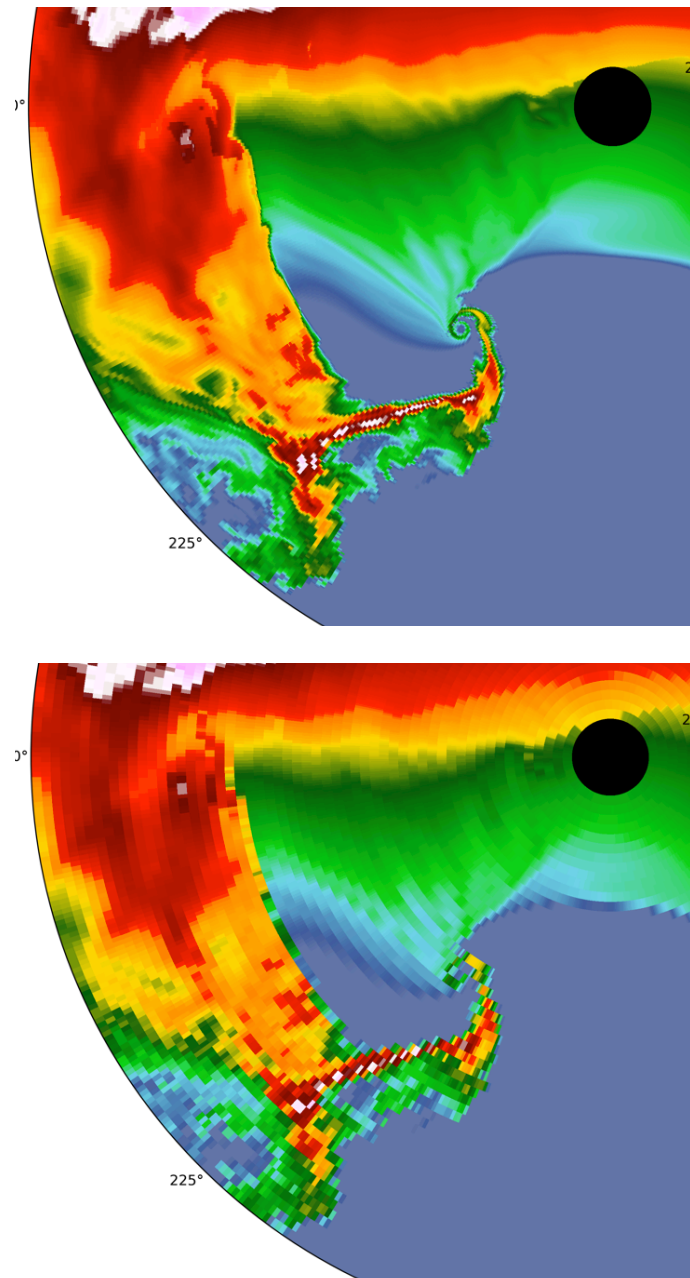


**Figure 13.** PPI scans of reflectivity at time 5550 at approximate RaXPol (upper) and WSR-88D (lower) resolution.

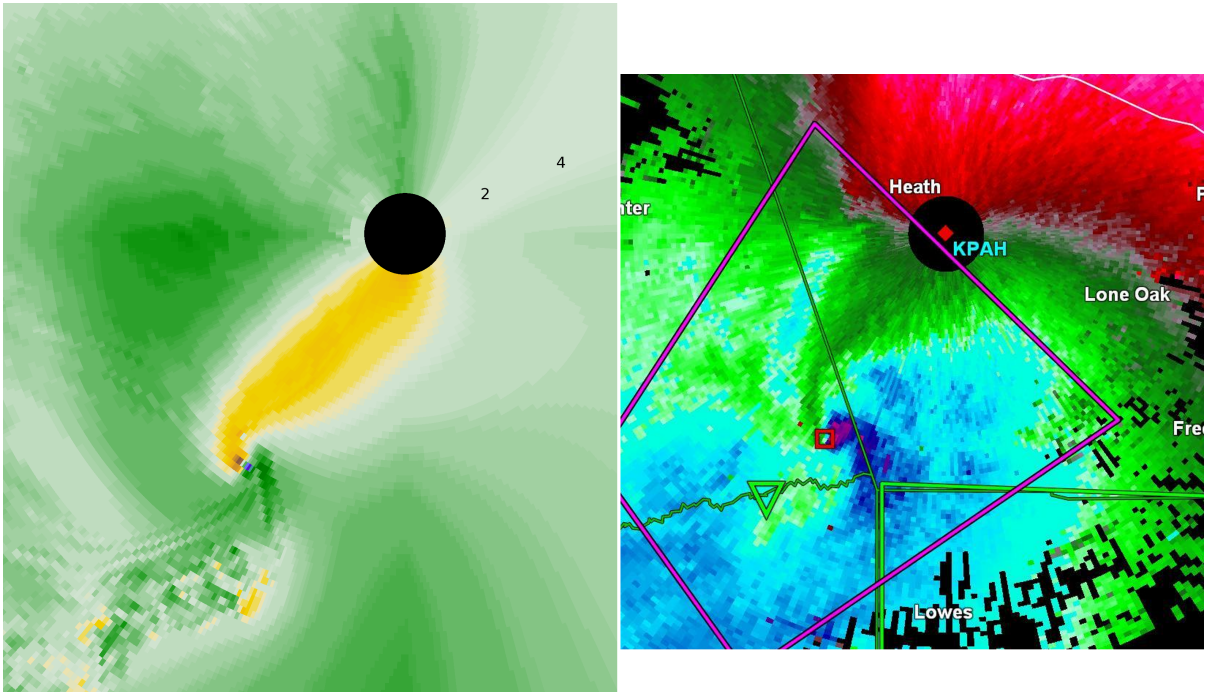


**Figure 15.** Emulated PPI scan of GRV at time 5550 (left) and a PPI scan of GRV from the KPAH radar site at the time of an ongoing EF-3 tornado (right). Black dots denote the radar location in both images. The pink polygon in the right image outlines the tornado warning, and the small red square is the location of the tornado.

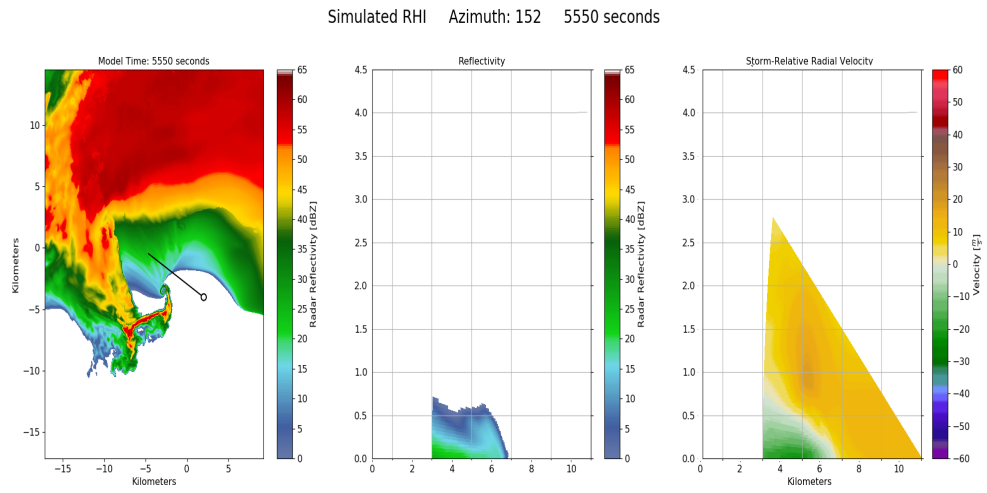


**Figure 16.** RHI scan perpendicular to the SVC at time 5550. Panels shown are same as figure 7.

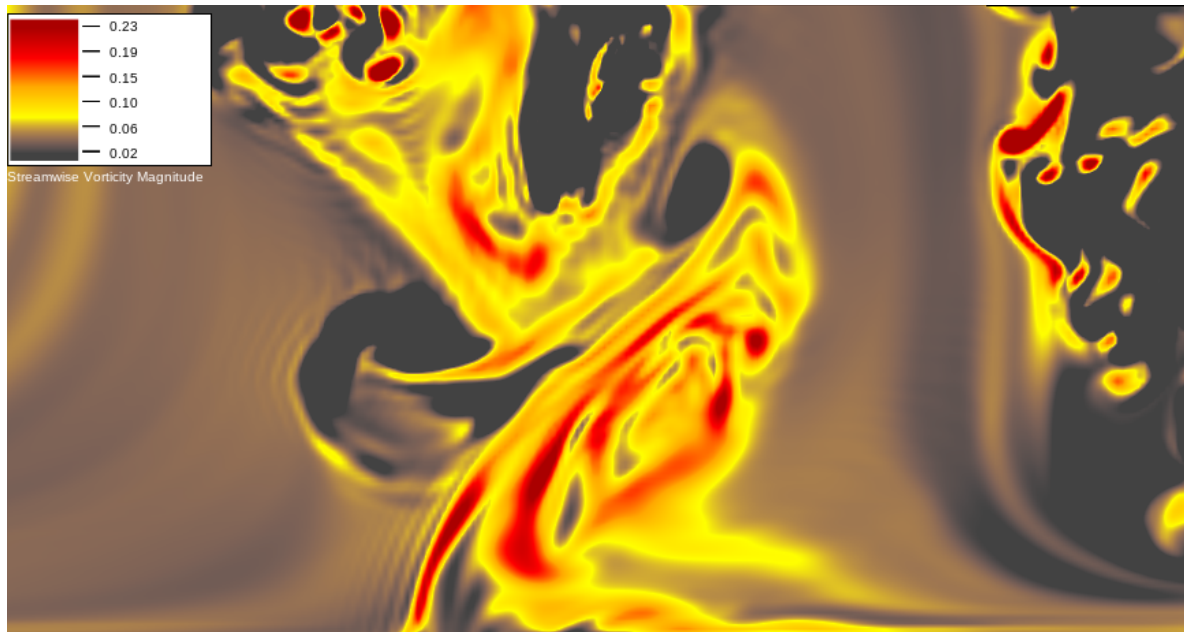


**Figure 17.** Horizontal cross section of model streamwise vorticity at time 3830 along the black line shown in figure 14.

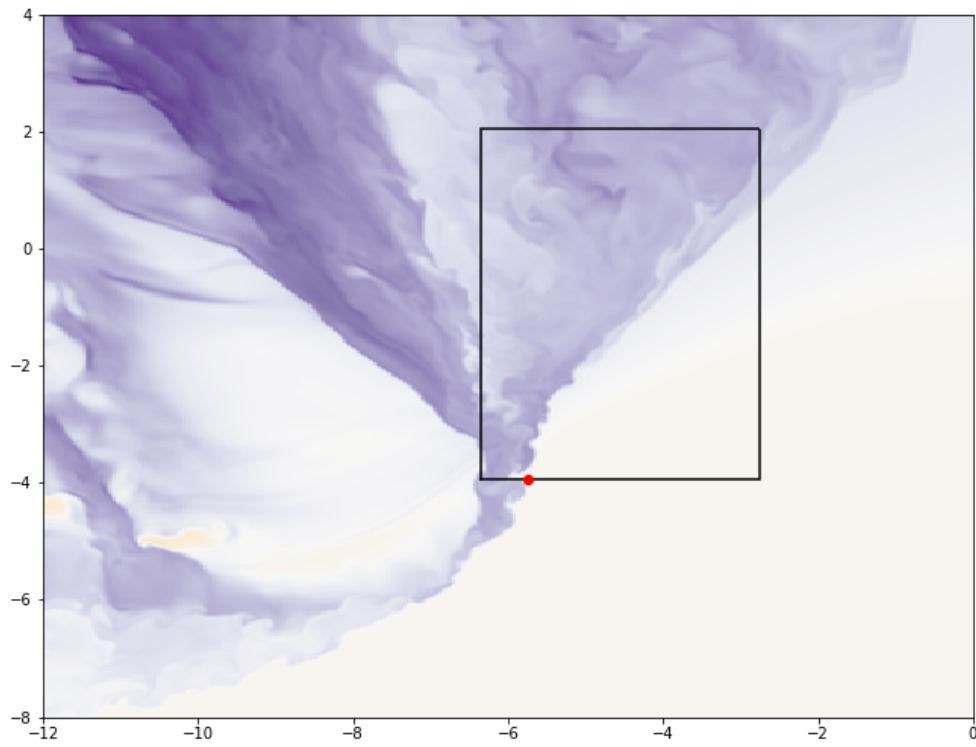


**Figure 18.** Potential temperature perturbation field with black box denoting area of averaging for time-height plots.

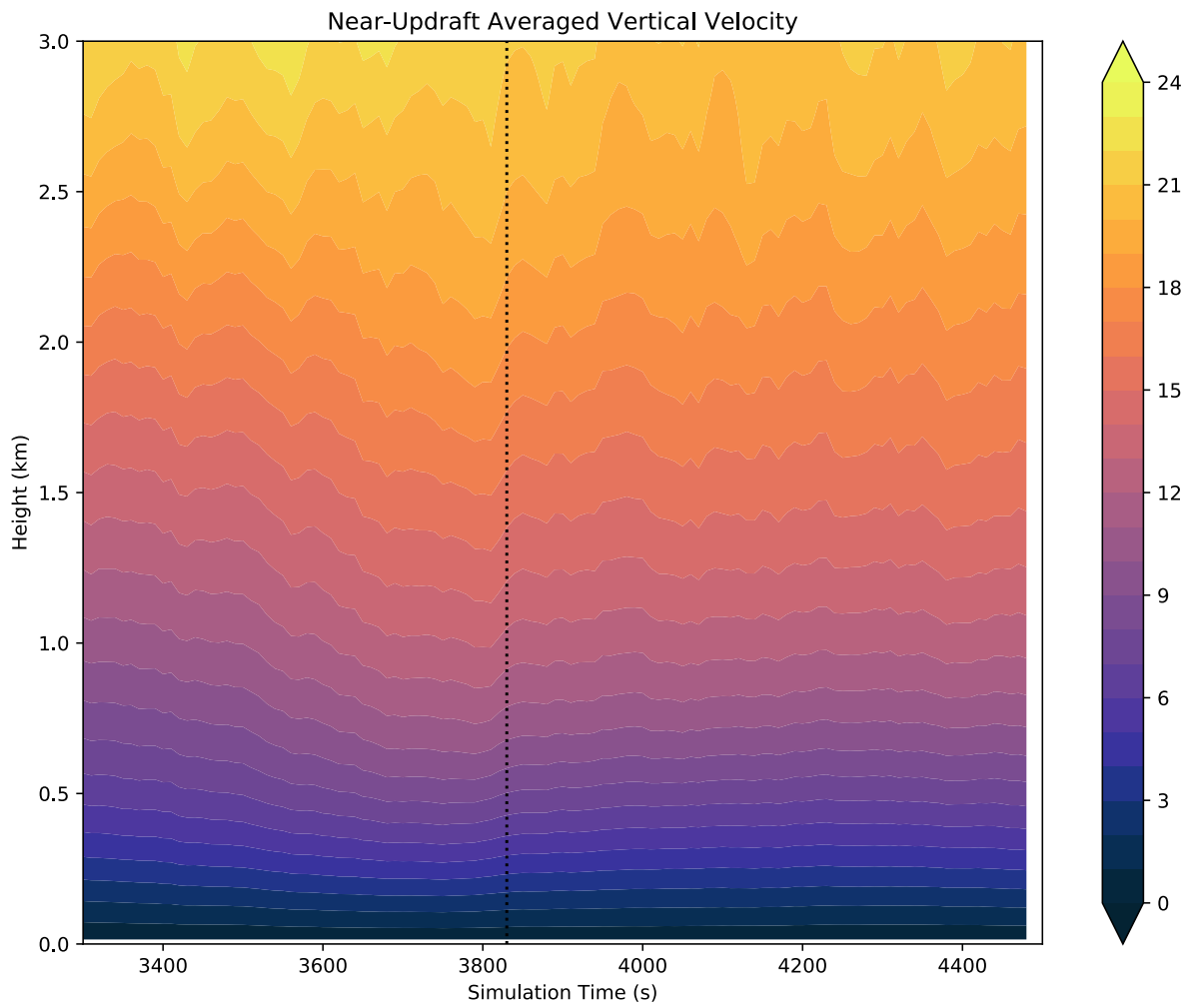


**Figure 19.** Time-height plot of near-updraft averaged vertical velocity over black box in Figure 16 with black dotted line denoting tornado genesis at time 3830.

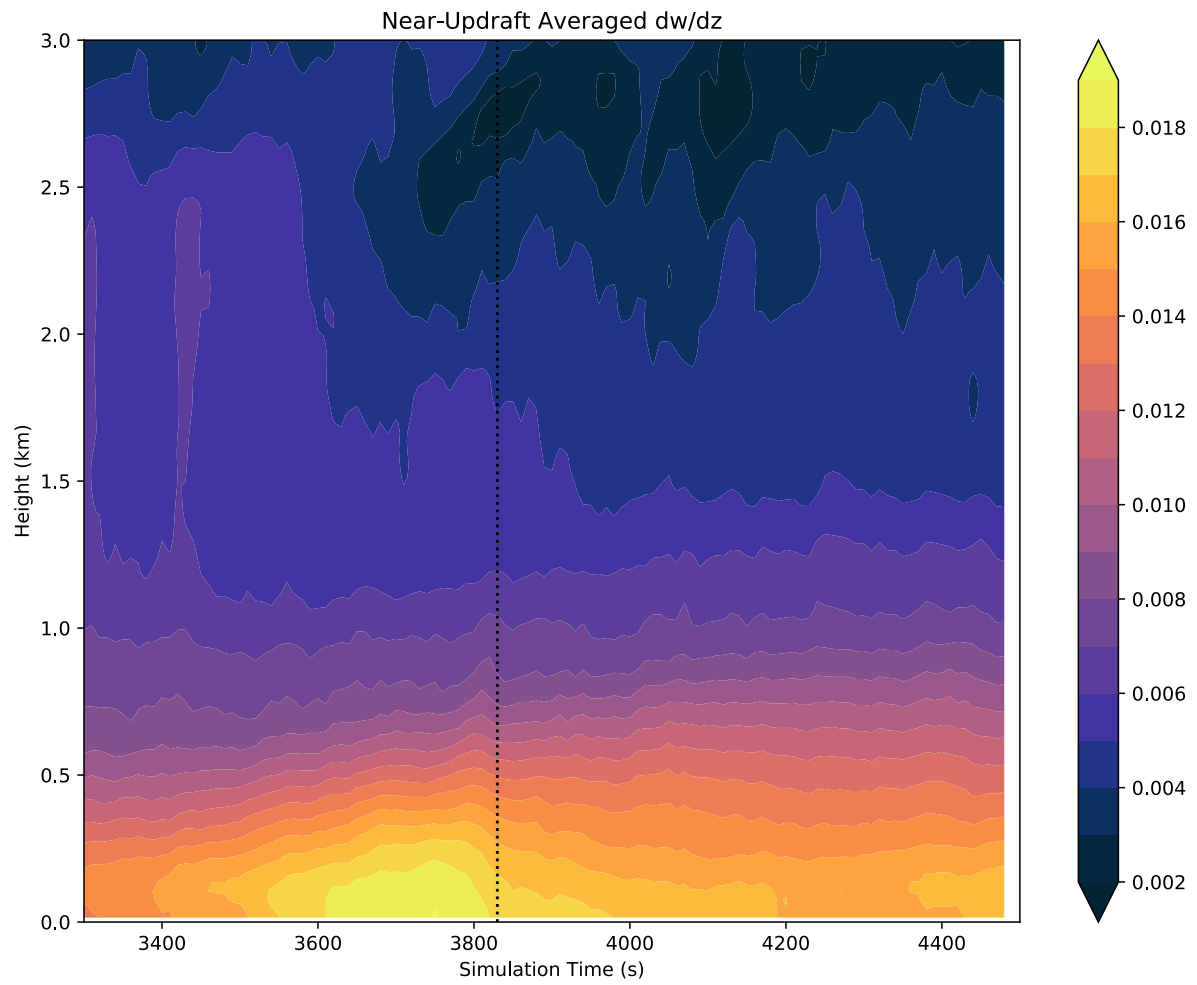


**Figure 20.** Same as Figure 17 but for near-updraft averaged  $dw/dz$ .

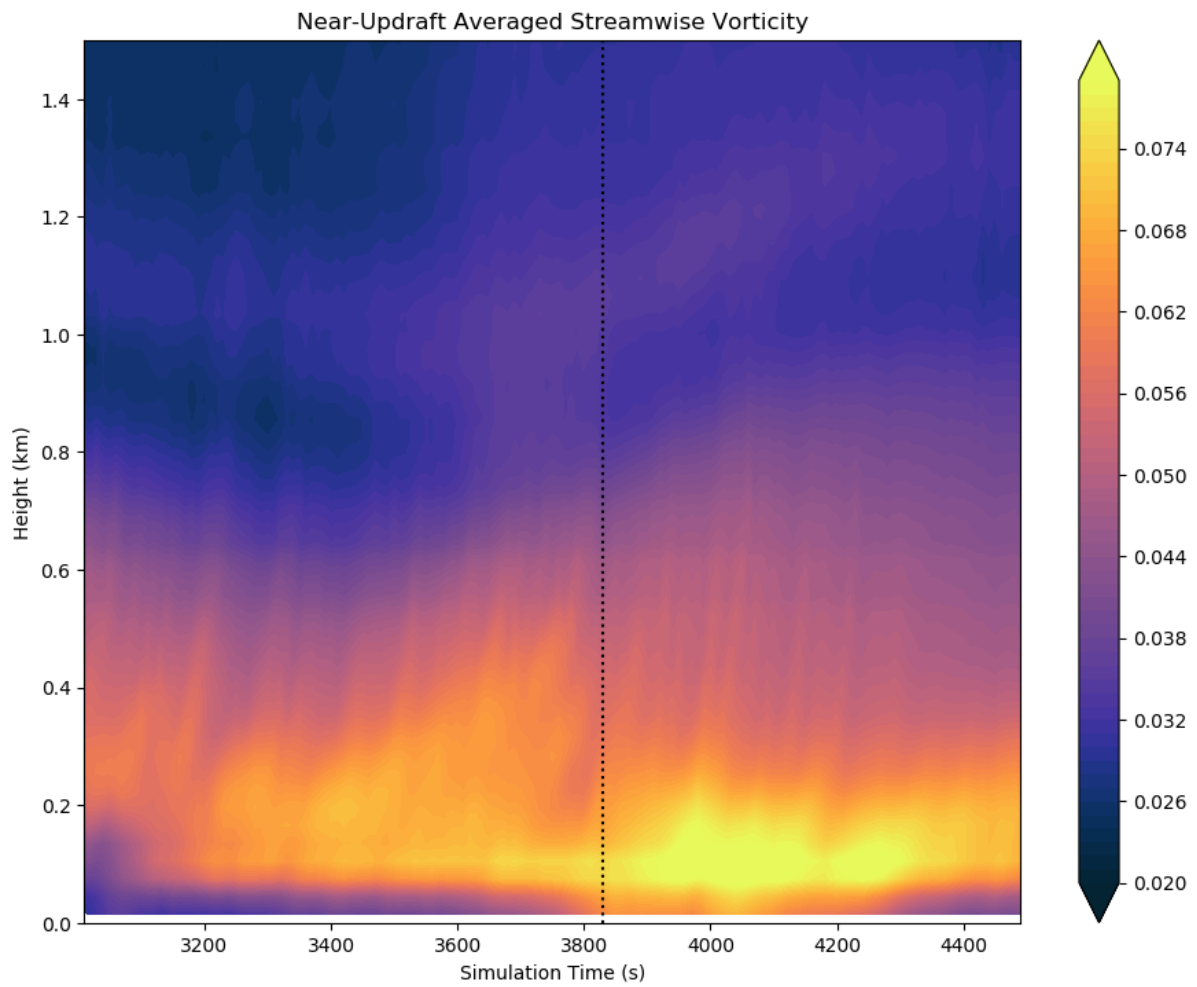


**Figure 21.** Same as Figure 17 but for near-updraft averaged streamwise vorticity.

## Bibliography

- Barnes, S. L., 1978: Oklahoma thunderstorms on 29–30 April 1970. Part I: Morphology of a tornadic storm. *Mon. Wea. Rev.*, **106**, 673–684.
- Brandes, E. A., 1981: Finestructure of the Del City-Edmond tornadic mesocirculation. *Mon. Wea. Rev.*, **109**, 635–647.
- Brandes, E. A., 1984: Relationships between radar-derived thermodynamic variables and tornadogenesis. *Mon. Wea. Rev.*, **112**, 1033–1052.
- Burgess, D. W., R. A. Brown, L. R. Lemon, and C. R. Safford, 1977: Evolution of a tornadic thunderstorm. Preprints, *10th Conf. on Severe Local Storms*, Omaha, NE, Amer. Meteor. Soc., 84–89.
- Fujita, T. T., 1975: New evidence from the April 3–4, 1974 tornadoes. Preprints, *Ninth Conf. on Severe Local Storms*, Norman, OK, Amer. Meteor. Soc., 248–255.
- Grzych, M. L., B. D. Lee, and C. A. Finley, 2007: Thermodynamic analysis of supercell rear-flank downdrafts from project ANSWERS. *Mon. Wea. Rev.*, **135**, 240–246.
- Isom, B., and Coauthors, 2013: The atmospheric imaging radar: Simultaneous volumetric observations using a phased array weather radar. *J. Atmos. Oceanic Technol.*, **30**, 655–675, doi:<https://doi.org/10.1175/JTECH-D-12-00063.1>.
- Kosiba, K. A., J. Wurman, Y. Richardson, P. Markowski, P. Robinson, and J. Marquis, 2013: Genesis of the Goshen County, Wyoming, tornado on 5 June 2009 during VORTEX2. *Mon. Wea. Rev.*, **141**, 1157–1181, doi:<https://doi.org/10.1175/MWR-D-12-00056.1>.
- Kurdzo, J.M., F. Nai, D.J. Bodine, T.A. Bonin, R.D. Palmer, B.L. Cheong, J. Lujan, A. Mahre, and A.D. Byrd, 2017: [Observations of Severe Local Storms and Tornadoes with the Atmospheric Imaging Radar](https://doi.org/10.1175/BAMS-D-15-00266.1). *Bull. Amer. Meteor. Soc.*, **98**, 915–935, <https://doi.org/10.1175/BAMS-D-15-00266.1>
- Markowski, P. M., 2002a: Mobile mesonet observations on 3 May 1999. *Wea. Forecasting*, **17**, 430–444
- Markowski, P. M., J. M. Straka, and E. N. Rasmussen, 2002: Direct thermodynamic observations within the rear-flank downdraft of nontornadic and tornadic supercells. *Mon. Wea. Rev.*, **130**, 1692–1721.
- Markowski, P. M., J. M. Straka, E. N. Rasmussen, R. P. Davies-Jones, Y. Richardson, and J. Trapp, 2008: Vortex lines within low-level mesocyclones obtained from pseudo-dual-Doppler radar observations. *Mon. Wea. Rev.*, **136**, 3513–3535,
- Markowski, P. M., and Y. P. Richardson, 2014: The influence of environmental low-level shear and cold pools on tornadogenesis: Insights from toy simulations. *J. Atmos. Sci.*, **71**, 243–275,

Markowski, P., Y. Richardson, and G. Bryan, 2014: [The Origins of Vortex Sheets in a Simulated Supercell Thunderstorm](https://doi.org/10.1175/MWR-D-14-00162.1). *Mon. Wea. Rev.*, **142**, 3944–3954, <https://doi.org/10.1175/MWR-D-14-00162.1>

Marquis, J., Y. P. Richardson, P. M. Markowski, D. C. Dowell, and J. Wurman, 2012: Tornado maintenance investigated with high-resolution dual-Doppler and EnKF analysis. *Mon. Wea. Rev.*, **140**, 3–27, doi:<https://doi.org/10.1175/MWR-D-11-00025.1>.

Pazmany, A.L., J.B. Mead, H.B. Bluestein, J.C. Snyder, and J.B. Houser, 2013: [A Mobile Rapid-Scanning X-band Polarimetric \(RaXPo\) Doppler Radar System](https://doi.org/10.1175/JTECH-D-12-00166.1). *J. Atmos. Oceanic Technol.*, **30**, 1398–1413, <https://doi.org/10.1175/JTECH-D-12-00166.1>

Rotunno, R., 2013: The fluid dynamics of tornadoes. *Annu. Rev. Fluid Mech.*, **45**, 59–84, doi:<https://doi.org/10.1146/annurev-fluid-011212-140639>.

Rotunno, R. and J.B. Klemp, 1982: [The Influence of the Shear-Induced Pressure Gradient on Thunderstorm Motion](https://doi.org/10.1175/1520-0493(1982)110<0136:TIOTSI>2.0.CO;2). *Mon. Wea. Rev.*, **110**, 136–151, [https://doi.org/10.1175/1520-0493\(1982\)110<0136:TIOTSI>2.0.CO;2](https://doi.org/10.1175/1520-0493(1982)110<0136:TIOTSI>2.0.CO;2)

Schueth, A. 2018, 'Comparing Observations and Simulations of the Streamwise Vorticity Current in Tornadoic and Nontornadoic Supercells', *The 29<sup>th</sup> Conference on Severe Local Storms*, American Meteorological Society, Stowe, VT.

Straka, J. M., E. N. Rasmussen, and S. E. Fredrickson, 1996: A mobile mesonet for fine-scale meteorological observations. *J. Atmos. Oceanic Technol.*, **13**, 921–936.

Straka, J. M., E. N. Rasmussen, R. P. Davies-Jones, and P. M. Markowski, 2007: An observational and idealized numerical examination of low-level counter-rotating vortices toward the rear flank of supercells. *E. J. Severe Storms Meteor.*, **2** (8), 1–22.

Wakimoto, R.M., 1982: [The Life Cycle of Thunderstorm Gust Fronts as Viewed with Doppler Radar and Rawinsonde Data](https://doi.org/10.1175/1520-0493(1982)110<1060:TLCOTG>2.0.CO;2). *Mon. Wea. Rev.*, **110**, 1060–1082, [https://doi.org/10.1175/1520-0493\(1982\)110<1060:TLCOTG>2.0.CO;2](https://doi.org/10.1175/1520-0493(1982)110<1060:TLCOTG>2.0.CO;2)